Proceedings of the 28th IEEE
EMBS Annual International Conference
New York City, USA, Aug 30-Sept 3, 2006

Computer Modeling Provides a New Tool for Clinically Diagnosing Melanoma Spread through the Lymphatics

Hayley M. Reynolds, P. Rod Dunbar, R. F. Uren, and Nicolas P. Smith

Abstract—**In this study an anatomically accurate framework is presented to visualize clinical melanoma data in 3D. Sentinel lymph node biopsy (SLNB) data from the Sydney Melanoma Unit (SMU) has been used, where each patient's primary cutaneous melanoma site and corresponding sentinel lymph node locations have been recorded.**

Anatomically accurate finite element geometries of the skin and lymph nodes have been created using the Visible Human dataset. SMU's full SLNB database has been mapped from 2D onto this 3D anatomical framework via free-form deformation and projection techniques. Spatial statistical analysis and heat map displays have been calculated and visualized relating melanoma sites on the skin to sentinel lymph node fields.

These detailed spatial maps provide the first anatomically accurate link between skin sites and lymphatic drainage. The extension and ongoing application of this work in the clinic is a novel method to capture data for both improved melanoma diagnosis and a better understanding of lymphatic drainage in the body.

I. Introduction

MELANOMA is the most serious form of skin cancer. It is a very aggressive tumor that can spread quickly throughout the body. Cutaneous melanoma begins in the epidermis of the skin appearing as an unusual freckle or mole, termed the 'primary melanoma'. Over time and without treatment melanoma can spread deeper into the skin and enter the lymphatic system to create secondary tumors in lymph nodes. Detection of melanoma cells in the lymph nodes is one of the earliest signs that the cancer has spread.

A sentinel lymph node biopsy (SLNB) is a technique used to determine whether melanoma has metastasized to lymph nodes, by biopsying the first nodes that cancer cells will reach. These nodes are termed sentinel nodes (SN), and are best defined as 'any lymph node receiving direct lymphatic drainage from a lesion site' [1]. Lymphatic mapping via lymphoscintigraphy (LSG) imaging is used to locate the SNs, as shown in Figure 1. A radioactive tracer is injected into the skin around the primary melanoma, and this tracer is tracked as it drains to the SNs. These nodes are then surgically removed and examined for tumor. The histological results will highly influence a patient's prognosis.

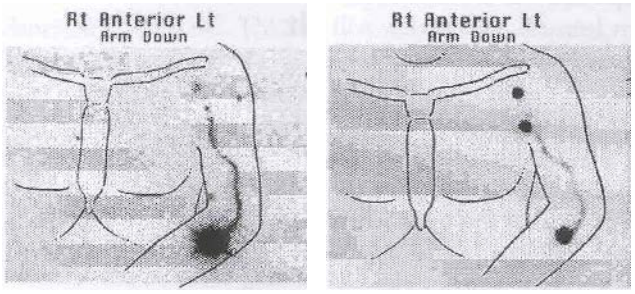

(a) (b)

Fig. 1. LSG images of patient with primary melanoma on their forearm [2]. (a) Early imaging (10 mins post injection) tracks the lymph vessel draining the skin site. (b) Late imaging (2½ hrs post injection) shows two SNs located in the axilla.

LSG imaging has shown that lymphatic drainage of the skin is highly variable between patients [3]. This means that melanoma does not spread in a clinically predictable manner.

The Sydney Melanoma Unit (SMU) helped pioneer the SLNB technique and has the world's largest database of over 5000 treated patients. Previously there was no good way to visualize this data in 3D for clinical use. This study presents an anatomically based technique to visualize clinical data relating primary melanoma sites to sentinel lymph nodes. This provides important clinical information when full LSG mapping is not available or practical.

II. Methodology

A. Skin Model Construction

High resolution axial slices of the Visible Human male [4] provided the required anatomical data used to generate a 3D geometric model of the human skin. The following steps were carried out to create the skin mesh:

1) *Data Digitization*: The skin surface was located visually on each VH image and digitized to create a 3D data cloud from stacked 2D slices (Figure 2a).
2) *Initial Linear Mesh*: An initial linear mesh was created by selecting data points from the digitized data cloud at regular intervals. These selected data points were used as

Manuscript received April 24, 2006. This work was supported by the Centre of Molecular Biodiscovery, a New Zealand Centre of Research Excellence in Biology and Biomedicine (CMB CoRE).

H. M. Reynolds is a PhD student at the Bioengineering Institute, University of Auckland, New Zealand (phone: 64-9-373-7599 ext. 89560; e-mail: h.reynolds@auckland.ac.nz).

P. R. Dunbar is with the School of Biological Sciences, University of Auckland, New Zealand. (e-mail: r.dunbar@auckland.ac.nz).

R. F. Uren is with the Discipline of Medicine, University of Sydney, Sydney, Australia. (e-mail: ruren@mail.usyd.edu.au).

N. P. Smith is with the Bioengineering Institute and Engineering Science Department, University of Auckland, New Zealand. (e-mail: np.smith@auckland.ac.nz).

nodes to create linear finite elements in Rectangular Cartesian coordinates to approximate the skin surface.

3) *Fitting*: A bicubic slope continuous finite element mesh was created from the initial linear mesh by fitting the data points via the application of a non-linear fitting process [5]. This process is cast as minimizing the least-squares distance function F between the data points and their projections onto the linear mesh. F is defined as:

$$F(\mathbf{u}_n) = \sum_{d=1}^{N} \left\| \mathbf{u}(\xi_{1d}, \xi_{2d}) - \mathbf{z}_d \right\|^2 + F_s(\mathbf{u}_n) \qquad (1)$$

where **u** is the vector of interpolated coordinates which is a function of the fitted nodal values. $\boldsymbol{\xi}_d$ are the local material coordinates for each data point calculated from the orthogonal projection of the data onto the mesh. $\mathbf{z}_d$ are the global coordinates of the data points, F_s is a Sobelov smoothing penalty function of the mesh derivatives and $\mathbf{u}_n$ is introduced to maintain smoothness of the mesh where data is noisy or insufficient.

The skin model (Figure 2b) has been constructed with 842 nodes and 886 elements, and has an RMS error of 2.29mm

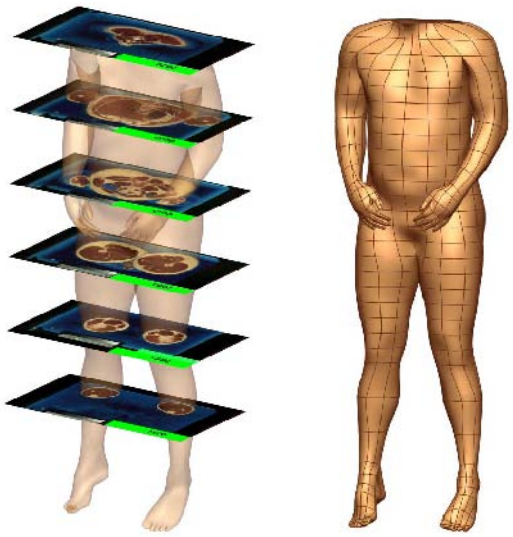

(a) (b)

Fig. 2. Construction of the finite element skin mesh. (a) Stacked 2D Visible Human images used to digitize the skin. (b) Fitted skin mesh.

B. Lymph Node Model Construction

Lymph nodes are small bean-shaped structures, usually between 0.1 – 2.5cm long. Large numbers are found in the groin, armpit and abdominal areas. Recognized generic regions where nodes are located are called lymph node fields. The SMU defines 43 different node fields that drain the skin, and each field has been defined in the model as shown in Figure 3.

Often lymph nodes were difficult to visually locate on VH images due to their small size. Therefore their geometric positions have been determined using a combination of digitizing VH images, and positioning the nodes relative to anatomical structures such as blood vessels and muscles as described in the literature [6,7,8].

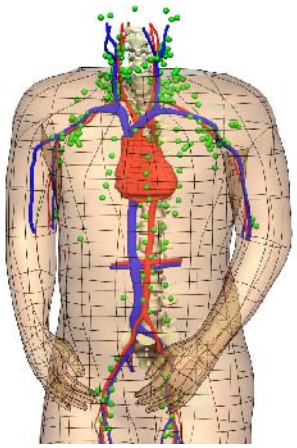

Fig. 3. Model of the lymph node fields that drain the skin. Note that the popliteal lymph nodes behind the knees are not visible in this image.

C. Mapping Clinical Data

Clinical SLNB data at the SMU has been recorded in 2D, therefore mapping was required to transform the data onto the 3D anatomical model. Each patient's primary melanoma site on the skin has been recorded in as an *(X,Y)* coordinate on one of six body outline maps. The body outline views are of the anterior and posterior torso, anterior and posterior legs, and left and right lateral head.

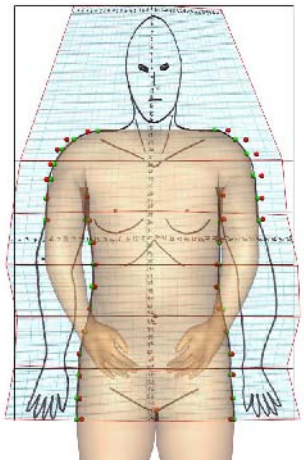

Fig. 4. Body outline of the anterior torso host-mesh fitted to align with the 3D skin model. Landmark points are shown in red and target points in green. Note that the arms and head have been treated separately.

The torso and leg body outlines have been morphed to align with the skin model using a 'free-form' deformation technique called 'host-mesh' fitting [9]. This process enables a finite element model to be customized to a specific set of data, by minimizing the distance between a set of landmark (initial) and target (final) points. The mesh that is transformed, called the 'slave-mesh' is completely embedded within a 'host-mesh'.

The host-mesh is deformed to minimize the distance between the landmark and target points, calculated using Equation 1. In this case $\mathbf{z}_d$ are the global target points and $\mathbf{u}(\xi_{1d},\xi_{2d},\xi_{3d})$ are the interpolated landmark points, extended to 3D for a volume host-mesh. Subsequently the slave-mesh will also deform along with the host-mesh, and the new slave-mesh coordinates can be interpolated.

Figure 4 shows the anterior torso body outline morphed to align with the anterior view of the skin mesh, where landmark points were digitized from the body outlines and the target points from the 3D skin model. A tri-linear host-mesh has been used to surround the bilinear body outline slave-mesh.

After host-mesh fitting, each melanoma coordinate has been updated relative to the deformed body outline and projected orthogonally in the y-direction onto the skin mesh (Figure 5). To enable direct orthogonal projection the skin model has been 'deflated' from 3D to 2D, by setting all y-coordinates of the skin model and their derivatives to zero. The local coordinates of each melanoma site projected onto the 2D skin mesh was used to calculate the 're-inflated' melanoma coordinates on the 3D bicubic skin mesh as shown in Figure 6.

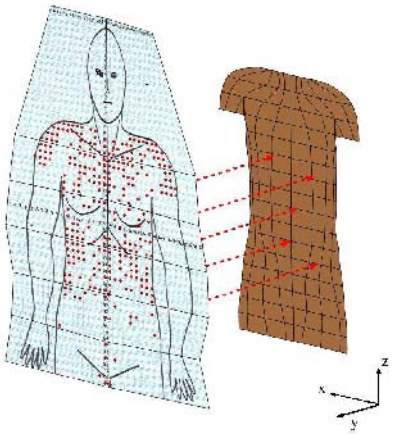

Fig. 5. Projecting melanoma coordinates from anterior torso body outline onto the 'flattened' 2D skin mesh. The full database of melanoma coordinates on the anterior torso are shown.

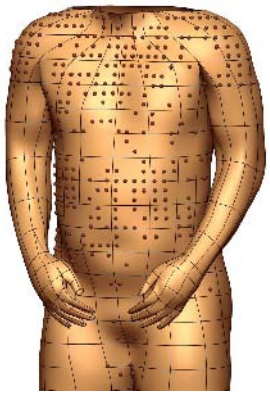

Fig. 6. Anterior torso melanoma coordinates on the 3D skin model.

The arms, hands and feet of the skin model were in a different orientation to the body outlines and therefore direct orthogonal projection was not possible. The VH dataset used to create the skin mesh has the arms oriented anterior to the body, while the body outlines orient the arms lateral to the body. Therefore the skin model's arms have been moved via host-mesh fitting relative to a rigid-body translation of bones at the elbow joint, as shown in Figure 7a. A tri-linear host-mesh has been used, and landmark and target points taken from the surface of the ulna and radius bones.

Melanoma points on the arms have been projected by separating the skin mesh into anterior and posterior arm segments; converting these arm segments from 3D into 2D; projecting the melanoma coordinates orthogonally onto them; and then recalculating the coordinates on the 3D skin model. The feet and hand melanoma sites have been placed onto the model manually.

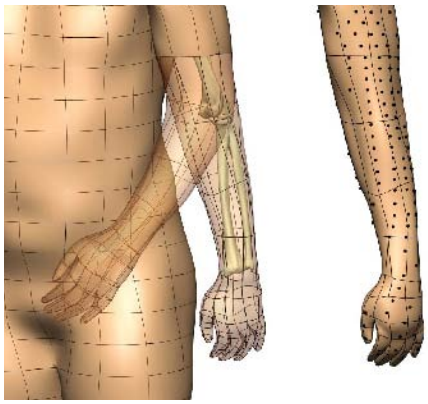

(a) (b)

Fig. 7. (a) Host-mesh fitting the left arm lateral to the body. (b) Melanoma points on the left arm and hand.

SN locations for each melanoma patient have been recorded at the SMU as a code according to the node field it was located in. For example, a patient with SNs in the left axilla and left inguinal node fields will have node field codes recorded as 'la' and 'li'. SN locations could not be projected directly onto the model since spatial information has not been recorded in a generic manner. In the absence of exact SN locations, the lymph node model has been reduced to one representative node in each nodefield, onto which SNs have been mapped.

III. Results

Spatial statistical analysis of the data has been conducted, investigating melanoma sites based on sentinel lymph node fields and vice versa.

Fields have been fitted on the skin model to visualize the likelihood that a primary melanoma site on the skin will drain to a particular node field. Figure 8 shows the percentage likelihood that a melanoma will drain to the left axillary node field based on 1639 patient cases in the database. It shows that patients with melanomas on their left arm or left torso above the umbilicus will almost certainly

have a SN in this node field. This display also quantitatively shows that lymphatic drainage of the skin can occur to contralateral node fields.

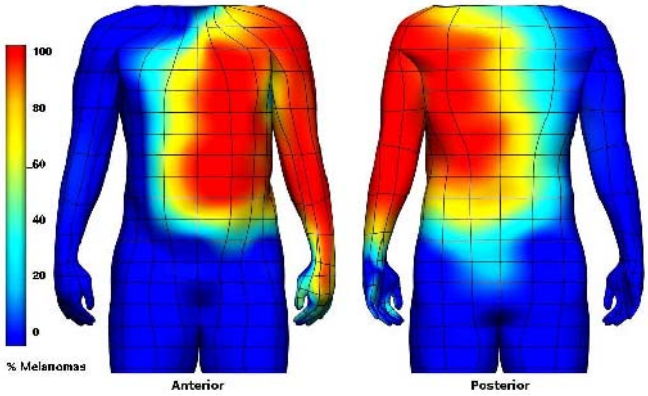

Fig. 8. Heat map displaying the percentage likelihood that a primary melanoma site will drain to SNs in the left axillary node field.

Displaying lymph node fields that will potentially contain SNs based on primary melanoma sites have also been visualized. Figure 9 demonstrates the utility of a clinical and educational tool developed as part of this study. It provides the ability to select skin elements and display the potential draining lymph node fields with a percentage likelihood calculated from all previous cases.

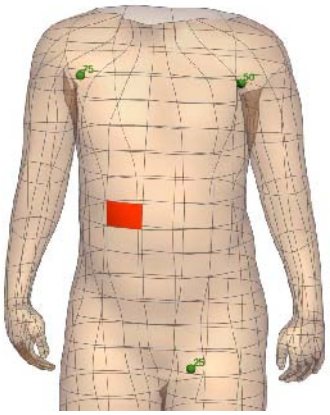

Fig. 9. Potential SN sites based on a region of skin on the torso. From previous patient data, 75% have had lymphatic drainage to the right axilla, 50% to the left axilla and 25% to the left inguinal node fields.

IV. Discussion

Currently the skin model does not include the head or neck which can often develop melanoma. Future extension of this work will be to create a head and neck skin mesh.

V. Conclusions & Future Work

These detailed spatial maps provide the first anatomically accurate link between skin site and lymphatic drainage. The extension and ongoing application of this work is to incorporate these novel displays of SLNB data into a software tool that will be made available to clinicians. As a result melanoma diagnosis and treatment will be improved, thereby aiding doctors and their patients fight against this fatal disease.

Acknowledgment

The authors gratefully acknowledge Professor John Thompson from the Sydney Melanoma Unit for his clinical input. H. M. Reynolds thanks her colleagues at the Bioengineering Institute for their contributions and the Center for Molecular Biodiscovery for their financial support.

References

[1] R. F. Uren, R. Howman-Giles, J. F. Thompson, et. al., "Lymphoscintigraphy to identify sentinel nodes in patients with melanoma", *Melanoma Res*., vol. 4, pp. 395-399, 1994.

[2] J. F. Thompson and R. F. Uren, "Teaching Points on Lymphatic Mapping for Melanoma from the Sydney Melanoma Unit," *Semin. Oncol.*, vol. 31, no. 3, pp. 349 – 356, 2004.

[3] R.F. Uren, J.F. Thompson, and R. Howman-Giles, *Lymphatic drainage of the skin and breast: locating the sentinel nodes*, Harwood Academic Publishers, Amsterdam, 1999.

[4] M. J. Ackerman, "The visible human project," *Proc IEEE,* vol. 86, pp. 504 – 511, 1998.

[5] C. P. Bradley, A. J. Pullan, and P. J. Hunter, "Geometric modeling of the human torso using cubic hermite elements," *Ann. Biomed. Eng*., vol. 25, pp. 96 – 111, 1997.

[6] P. L. Williams, R. Warwick, M. Dyson, and L. H. Bannister. *Gray's Anatomy*, 37 edn, Churchill Livingston, 1989.

[7] F. H. Netter, *Atlas of human anatomy*, 3 edn, ICON Learning Systems, 2003.

[8] C. D. Clemente, *Anatomy: A Regional Atlas of the Human Body,* 4 edn, Williams and Wilkins, Maryland, 1997.

[9] J. W. Fernandez, P. Mithraratne, S. F. Thrupp, M. H. Tawhai, and P. J. Hunter, "Anatomically based geometric modelling of the musculo-skeletal system and other organs," *Biomech. Model. Mechan.*, 2(3), 139 – 155. 2004.